crystals

MDPI

Article

Laser Written Stretchable Diffractive Optic Elements in Liquid Crystal Gels

Bohan Chen *, Zimo Zhao, Camron Nourshargh, Chao He, Patrick S. Salter, Martin J. Booth, Steve J. Elston and Stephen M. Morris *

Department of Engineering Science, University of Oxford, Parks Road, Oxford OX1 3PJ, UK
* Correspondence: bohan.chen2@eng.ox.ac.uk (B.C.); stephen.morris@eng.ox.ac.uk (S.M.M.)

Abstract: Direct laser writing (DLW) in liquid crystals (LCs) enables a range of new stimuli-responsive functionality to be realized. Here, a method of fabricating mechanically tunable diffraction gratings in stretchable LC gels is demonstrated using a combination of two-photon polymerization direct laser writing (TPP-DLW) and ultraviolet (UV) irradiation. Results are presented that demonstrate the fabrication of a diffraction grating that is written using TPP-DLW in the presence of an electric field in order to align and lock-in the LC director in a homeotropic configuration. The electric field is subsequently removed and the surrounding regions of the LC layer are then exposed to UV light to freeze-in a different alignment so as to ensure that there is a phase difference between the laser written and UV illuminated polymerized regions. It is found that there is a change in the period of the diffraction grating when observed on a polarizing optical microscope as well as a change in the far-field diffraction pattern when the film is stretched or contracted. These experimental results are then compared with the results from simulations. The paper concludes with a demonstration of tuning of the far-field diffraction pattern of a 2-dimensional diffraction grating.

Keywords: direct laser writing; diffraction gratings; stretchability; liquid crystals

Citation: Chen, B.; Zhao, Z.; Nourshargh, C.; He, C.; Salter, P.S.; Booth, M.J.; Elston, S.J.; Morris, S.M. Laser Written Stretchable Diffractive Optic Elements in Liquid Crystal Gels. *Crystals* **2022**, *12*, 1340. https://doi.org/10.3390/cryst12101340

Academic Editor: Ingo Dierking

Received: 11 August 2022
Accepted: 30 August 2022
Published: 22 September 2022

1. Introduction

Diffraction gratings are optical components with precisely defined periodic structures that are designed to manipulate the spatial distribution of light [1]. For example, they can split a beam of light into a number of diffracted beams or direct a beam into one specific order. Diffraction gratings play an important role in a number of applications including monochromators, spectrometers, augmented reality (AR)/virtual reality (VR) displays, wavefront measurements, beam steering, structured light and optical encoders for high precision motion control [2–8]. The development of switchable and tunable diffraction gratings is also of considerable interest for potential future wearable technologies [9].

Tuning a diffraction grating often relies on applying some form of external stimuli to alter the optical properties of the material or the architecture of the grating. This external stimulus might be, for example, in the form of an electric field, a change in the temperature, or a change in the humidity conditions [10,11]. With the advent of wearable and conformable photonics technologies, there is a particular interest in using strain or mechanical deformation to tune photonic devices [9,12–17]. Towards this end, there are a range of materials that exhibit a reversible elastic response to mechanical strain [18–33], such as polydimethylsiloxane (PDMS), polyethylene terephthalate (PET), polyimide and Parylene-C, which would potentially enable the grating to be deformed by introducing external tensile strain leading to tuning of the optical diffraction pattern [16,34–39].

Two-photon direct laser writing (TPP-DLW) is a popular microfabrication technique as it enables small structures (of the order of microns and less) to be fabricated in a range of materials and has proved to be a particularly powerful fabrication tool for the development of a range of different metamaterial and nanophotonic platforms [40–42]. Liquid crystal

(LC) gels are a material that exhibit both elasticity and long range orientational order of the molecules (characterized by a unit vector referred to as the director). Using laser writing to structure and impart new functionality in polymerizable LC gels and elastomers has also attracted considerable interest in recent years [7,9,43–45]. For example, combining TPP-DLW with LC gels has enabled the development of a wide range of tunable stimuli-responsive components whose optical properties change when the material is subjected to an external stimulus, for example, LC microactuators, micro-soft robotic systems and LC sensors [46–49].

An advantage of using an LC gel compared with isotropic materials, such as photocurable polymer resins, is that these materials combine birefringence with the mechanical stretchability. Polymer-stabilized LCs also have the advantage of being able to lock-in and maintain any desired phase profile with the use of an external electric field and/or surface alignment [50]. By applying a voltage during fabrication, TPP-DLW can be used to lock-in different alignments of the director through photopolymerization so as to create a sculptured polymer network. After removing the voltage, and depending upon the relative lengthscales involved, the LCs in the non-polymerized regions tend to relax back to the initial alignment conditions leading to a spatially varying phase profile across the device [43]. Furthermore, compared with Si photolithography, TPP-DLW has the capability to build structures in three dimensions leading to more sophisticated architectures and multi-functional optical components [51–54]. Figure 1 shows examples of the functionality that can be unlocked using TPP-DLW in LC devices when an electric field is applied during fabrication. This includes the ability to hide features such as quick response codes [55], transport microparticles and generate microfluidics-inspired flow of boundaries between different topologically distinct states [56], fabricate tuneable diffractive optics elements in the form of diffraction gratings and computer-generated holograms [43,57], and the development of stretchable optical elements, which is the subject of this paper.

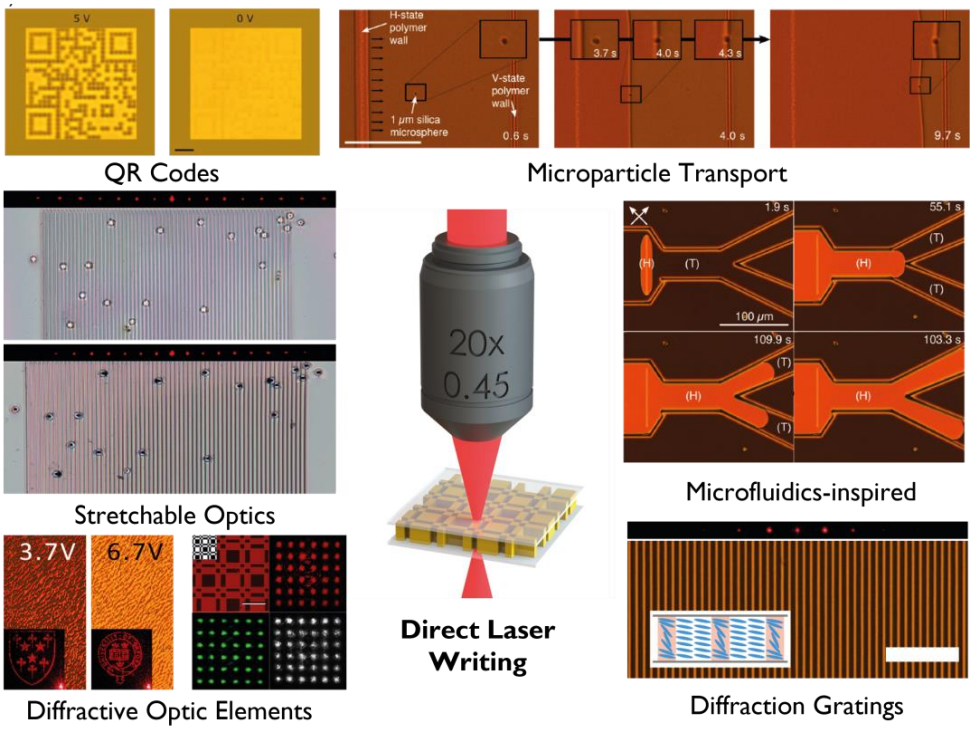

Figure 1. The range of functionality that our group has demonstrated using TPP-DLW in LC devices when an electric field is applied during fabrication [43,55–57]. This includes the development of switchable QR codes [55], microparticle transport and microfluidics inspired flow of defect walls [56], and diffractive optic elements in the form of one-dimensional diffraction gratings, Dammann gratings, and computer-generated holograms [43,57]. The focus of this paper is to demonstrate how this technique can be used to develop mechanically tuneable diffractive optic elements.

In this paper, we present a strategy to fabricate a mechanically tunable phase grating using a combination of laser writing and ultraviolet (UV) illumination to trigger polymerization in a photopolymerizable LC gel. After describing the laser writing process and demonstrating how the laser writing conditions influence the morphology of the polymerized structures, the fabrication process employed to manufacture stretchable diffraction gratings in LC gels is demonstrated. Results are then presented that show tuning of the period of the diffraction grating and it is shown how the diffraction pattern in the far-field is changed when the LC gel is extended or contracted. The degree of tuning is discussed and, where possible, results from simulations are presented to compare with our experimental findings. To conclude, a mechanically tunable 2-dimensional phase grating is demonstrated, and the pros and cons of the approach presented herein are discussed.

2. Materials and Methods

2.1. Laser Writing Conditions

In both this work and our previous work on TPP-DLW laser writing in LCs, we have used a custom-built system which is shown in Supplementary Materials, Figure S1. The laser source was a Titanium: Sapphire femtosecond laser (Spectra-Physics Tsunami) emitting at λ = 780 nm that was excited by a diode-pumped solid-state CW laser (Spectra-Physics Millennia V) emitting at λ = 532 nm. The laser pulse width was 100 fs by mode-locking at a repetition of 80 MHz.

Before fabricating the gratings into the LC gels, we considered the impact of the laser writing conditions (i.e., power, scan speed, and fabrication voltage) on the resulting polymerized structures. Results from these characterizations are presented in Figure 2 (different fabrication voltages and laser intensity) and Figure 3 (different laser powers and scanning speeds for different orientations of the laser polarization relative to the rubbing direction of the LC device). The LC mixture that was used consisted of three elements: 69 wt.% of the nematic LC mixture, E7 (Synthon Chemicals Ltd.), 30 wt.% of the reactive mesogen RM257 (1,4-Bis-[4-(3-acryloyloxypropyloxy) benzoyloxy]-2-methylbenzene (Synthon Chemicals Ltd.)), and 1 wt.% of the Photoinitiator Irgacure 819 (Ciba-Geigy). The components were then added to an empty vial and left in an oven at 70–75 °C overnight to mix the components via thermal diffusion. In both characterization tests, the structures were fabricated in a glass cell with anti-parallel rubbed polyimide alignment layers and indium tin oxide (ITO) electrodes on the inner surfaces of both substrates (Instec-LC5.0). The cell gap was measured to be 4.9 μm from the interference fringes recorded on a UV-Vis spectrometer (Agilent 8454). The ITO transparent electrodes enable a uniform electric field to be applied to the sample during laser microfabrication and the rubbed polyimide alignment layers ensure that, in the absence of an external electric field, the LC director would be homogeneously (planar) aligned in the plane of the device with a pre-tilt angle of approximately 4°. The filled glass cells were then loaded into the TPP-DLW system for fabrication.

In the laser writing process, a high energy ultrafast pulse train was focused into the bulk of LC sample through an objective lens with a 0.45 NA so that two-photon absorption only occurred within a relatively small volume (voxel size: 1 μm in the lateral dimension and 7 μm in the axial direction) in order to cross-link the reactive mesogens via a free-radical polymerization reaction that freezes-in the LC alignment permanently. By moving the translation stage with respect to the laser focus, a 3-dimensional polymer network structure can be constructed in the LC film [32,33]. Diffusion of the polymer network means that the resulting polymer structures are often slightly larger than the voxel sizes quoted above. Our experience is that if there is overlap between the focal volume and the substrate, the polymer walls are strongly tethered to the substrate.

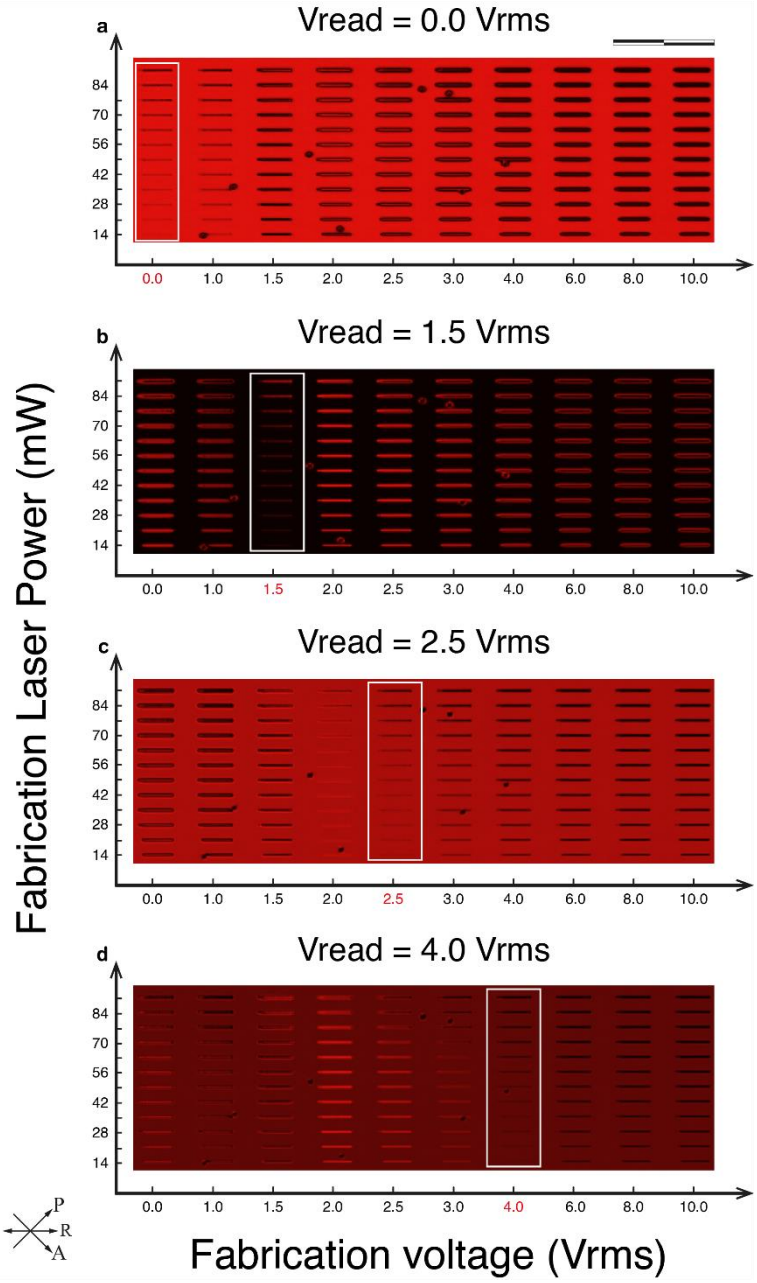

Figure 2. Laser written polymer walls in a polymerizable LC mixture for different fabrication laser powers and voltages applied to the LC during fabrication. The scale bar in the figure is 200 μm. The laser polarization was set to be perpendicular to the rubbing direction of the LC device. Images were recorded on a polarizing optical microscope when the rubbing direction was aligned at 45° to the transmission axes of the polarizer and analyzer pair, and with the aid of a narrow bandpass filter to remove all wavelengths beyond 640 nm–660 nm to avoid any further polymerization post-fabrication.

For the laser written polymerized structures shown in Figure 2, the voltage applied during the fabrication was varied (left to right on each subfigure) as was the laser power while the polarization was kept at an orientation that was perpendicular to the rubbing direction. Applying a voltage during fabrication causes a rotation out-of-plane of the LC director towards a homeotropic alignment at high voltages. Writing in the presence of a fabrication voltage causes the LC director alignment to be preserved at the moment of exposure to the laser writer. If, for example, the laser writing takes place with a large voltage applied, this results in a homeotropic alignment of the nematic LC being retained. The sample was translated at 100 μm/second during the fabrication process. Polarizing

optical microscope (POM) images of the structure were then taken with the device between a pair of crossed polarizers and the rubbing direction of the cell oriented at 45° to the transmission axes of the polarizers. Between each of the subfigures, the voltage applied during imaging (the read voltage) was varied. In the case when the read voltage is $V = 0$, there is a clear increase in the thickness of the lines as the writing voltage was increased. This is due to the elastic distortion of the LC. Away from the polymerized region, the director orientation is dictated by the alignment layers; within the polymerized region, the director orientation is determined by the writing voltage. The distance over which the director profile relaxes from the polymerized to the surface aligned orientation is dictated by the elastic constant of the LC and the orientation in the polymerized region. Hence, while changing the writing voltage does not impact the width of the polymerized lines, the lines appear wider due to the additional relaxation distance. Considering again the case where the read voltage was zero, we see that changing the writing voltage changes the intensity in the centre of the lines; this is a result of the retardance being fixed to a given value in the polymerized region. Increasing the writing power increased the contrast when the read voltage matched the write voltage. It also caused a slight increase in the line thickness when the read voltage did not match the write voltage.

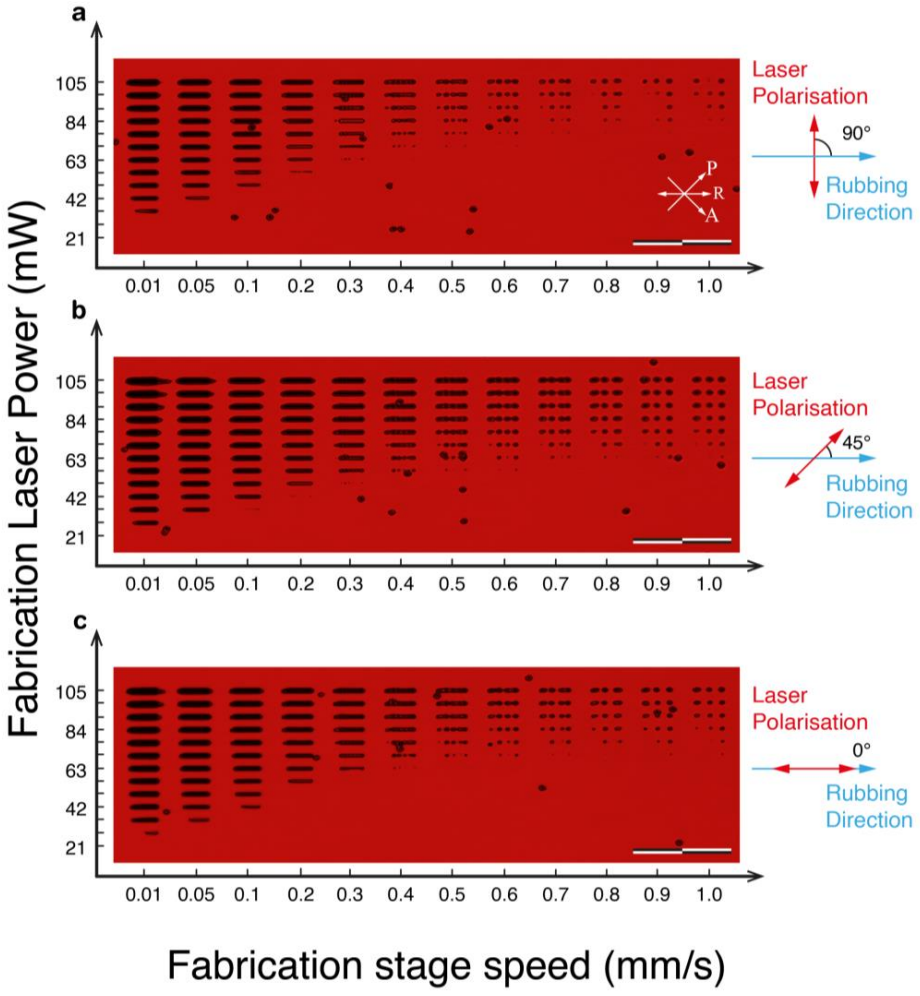

Figure 3. Laser written polymer walls in a polymerizable LC mixture for different fabrication laser powers and fabrication stage speeds when no voltage was applied to the LC during fabrication. Images were recorded on a polarizing optical microscope with an illumination source at 650 nm when the polarization of the writing laser was aligned at 90° (top), 45° (middle), or 0° (bottom) relative to the rubbing direction of the LC device. For these images, the rubbing direction was aligned at 45° to the transmission axes of the polarizer and analyzer pair and the scale bar in each image represents a length of 200 μm.

In Figure 3, the voltage applied during the writing process was fixed at 30 Vrms to ensure the LC was homeotropically aligned. Within each subfigure, the writing speed was then varied, and the laser power increased. The polarization of the writing laser relative to the rubbing direction was varied between each of the subfigures. The images were all taken with the LC glass cell between crossed polarizers, with a narrow bandpass filter at 650 nm after the illumination source to avoid any unwanted polymerization post-fabrication and with no voltage applied during inspection. Theoretically, if the laser is polarized perpendicular to the director, it only encounters the ordinary component of the refractive index. Otherwise, the laser should encounter a combination of the ordinary and extraordinary indices, which can cause a serious focal splitting aberration at a high numerical aperture [58]. However, according to the comparison in Figure 3, the polymer walls fabricated with different writing polarizations look qualitatively similar, primarily because the device is switched at a high voltage so it is effectively homeotropic and the aberration should be the same for all incident orientations of the laser linear polarizations. Furthermore, as the device here is quite thin (4.9 μm), the birefringent medium is contained purely within the laser focal intensity distribution, reducing the effect of the aberration. There is a noticeable increase in the linewidth when the laser power was increased, and when the writing speed was reduced, as both cause a greater exposure of the laser to the LC, which results in more polymerization. As the writing speed increases, we first see a reduction in the linewidth and then a breakup of the lines into discrete dots. These dots are smaller and more circular when the polarization is perpendicular to the rubbing direction which is again a result of the optical aberrations.

In practice, we tend to fabricate polymer structures at the maximum voltage that can safely be applied to the cell, as this always results in almost no in-plane retardance and hence shows some contrast at any voltage below this. We use a write speed of 0.1 mm/s as this is slow enough to allow smooth lines even at low powers, while not being so slow that the resolution suffers. Laser powers are typically chosen to be around 50 mW as this ensures that the polymer structures are fabricated consistently while again not causing a significant loss in resolution. These parameters are used herein for the fabrication of the diffractive optic elements in the stretchable LC gels. In the following, we describe the strategy employed in this work to fabricate phase gratings in LC gels using TPP-DLW and describe the steps taken to form a transparent stretchable free-standing film that preserves the phase grating once the LC film has been delaminated from glass substrates. Finally, the two experimental methods used in this work to characterize and analyze the stretchable gratings in the LC gel are discussed. Specifically, these two methods are: (1) direct observation of the grating on a POM and (2) observation of the diffraction pattern in the far-field.

2.2. Design and Fabrication of the Phase Grating

The configuration of our one-dimensional diffraction grating is illustrated in Figure 4. In this case, the low refractive index regions are defined by polymer walls of nematic LC that are homeotropically aligned and that have been frozen-in using the laser writing process in the presence of an electric field. The high refractive index regions, on the other hand, are defined by nematic LC regions between the homeotropic polymer walls that are then locked-in by subjecting the sample to UV illumination. To ensure that there is a phase difference between the high and low refractive index regions, the transmission as a function of voltage for the LC mixture was recorded (see Supplementary Figure S2) where it was found that the transmission reaches saturation at around 60 Vrms. Therefore, 100 Vrms was deemed more than sufficient to align the LC director homeotropically. After locking-in the low refractive index regions with the laser written localized polymer walls at 100 Vrms, the remaining LC-polymer mixture was then polymerized with UV light without a voltage to ensure that the polymer walls have a phase difference with the non-laser written regions.

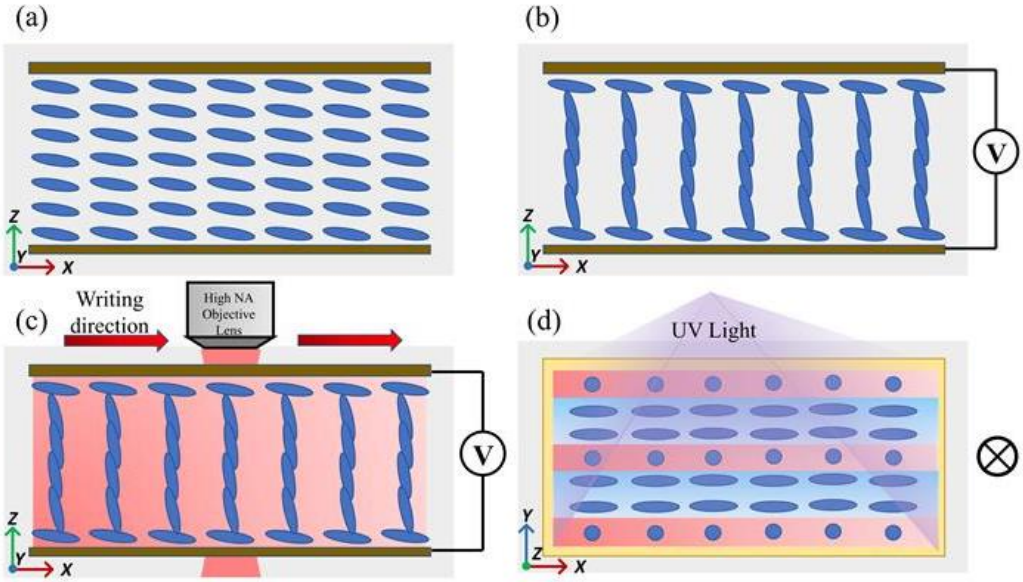

Figure 4. The one-dimensional phase grating fabricated using a combination of laser writing and ultraviolet (UV) illumination. (**a**) The nematic LC was homogeneously aligned such that the director lay in the plane of the glass cell with a pre-tilt at the substrate surfaces of 4°; (**b**) The illustration of the LC director switching to a homeotropic alignment with a voltage amplitude of 100 Vrms; (**c**) The laser writer scanned across the LC sample to form thin walls of polymer network along the *x*-direction that locked-in the homeotropic state; (**d**) After laser fabrication, the voltage was then removed and the sample was exposed to UV illumination to polymerize the remaining LC so as to freeze-in the alignment of the director between the polymer walls after the electric field had been removed. (**a**–**c**) show a side view of the LC between glass substrates while (**d**) shows a top view after UV polymerization where the pink regions correspond to the polymer walls for which the LC director was homeotropically aligned whereas the blue regions correspond to the bulk regions that have been polymerized using UV illumination and that consist of an LC director that was gradually relaxed from homeotropic alignment. The gratings were polarization dependent, which means that a diffraction pattern was only observed when the polarization of the incident light source was aligned parallel to the rubbing direction.

For the stretchable films, a 20 µm-thick glass cell (Instec-LC20.0) was used because the diffusion in the axial direction is sufficient to tether the polymer walls to the glass substrate. Here, the airgap represents not just the thickness of the LC layer between the glass substrates but also represents an approximate thickness for the free-standing film after the photopolymerization and delamination processes. The other properties of the glass cell (e.g., ITO layers, alignment layers etc.) were the same as that used in the previous section. The fabrication process for the stretchable phase gratings is illustrated in Figure 5. After capillary filling of the LC mixture (Figure 5a(ii)), the glass cells were then placed on a hotplate at 70 °C for several minutes to ensure that the LC mixture filled the cell uniformly. Finally, wires were attached to the glass cells using indium shot so that an electric field could be applied to the LC layer.

For this work, the TPP-DLW system was used to write a phase grating consisting of 65 parallel polymer walls with a 12 µm spacing between each polymer wall. Here, the laser written region was defined to be within the bulk of the LC layer, which then results in a polymer network that is denser in the center of the layer, but weaker close to the glass substrates. This leads to polymer structures that are tethered to the substrates and ensures that they do not drift or move even when the LC layer is subjected to an applied voltage. The fabrication accuracy in the *x*-*y* plane is less than 100 nm. Each polymer wall was written in the presence of a relatively high voltage (100 Vrms) with a power of 48 mW (Figure 5a(iii)) to ensure that a homeotropic alignment of the nematic LC had been obtained.

The reason why these parameters were chosen was that 65 polymer walls that are spaced at 12 µm intervals results in a grating with a total width of 768 µm, which is slightly larger than the laser diode spot diameter used to generate and inspect the diffraction patterns. A power of 48 mW was used for the laser writing process as this had been demonstrated to result in high fidelity polymer structures. A full list of the fabrication parameters used in this study is provided in Table S1 in the Supplementary Information.

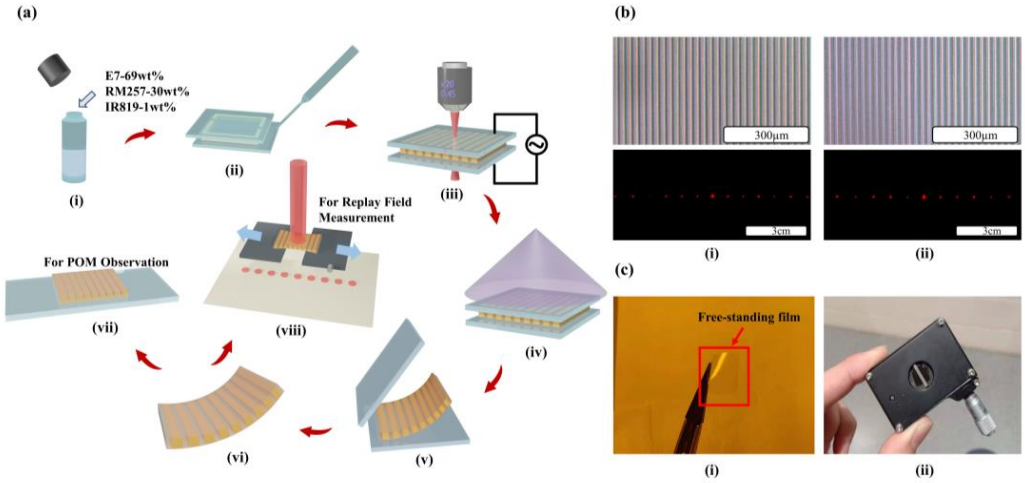

Figure 5. A stretchable one-dimensional diffraction grating in a liquid crystal (LC) gel. (**a**) Illustration of the fabrication and measurement process used to construct and characterize the mechanically stretchable grating: (i) mixture preparation, (ii) capillary filling of glass cell, (iii) fabrication of a 1-D diffraction grating with a voltage applied to the LC cell, (iv) bulk photo-polymerization of the film using ultraviolet illumination, (v) delamination of the cell to form a free-standing LC film that is approximately 20 µm thick, (vi) extraction of the flexible film, (vii) polarising optical microscope (POM) observation of the film, (viii) far (Replay) field observation of the diffraction pattern. (**b**) The POM (top) and far (replay)-field (bottom) images of the phase grating before (i) and after (ii) delamination. (**c**) Photographs of the LC free-standing film: (i) after delamination and (ii) mounted on an adjustable slit for stretchability and reversibility measurements.

After the formation of the phase grating, the samples were then illuminated with UV light to trigger polymerization in the remaining unreacted regions of the sample (Figure 5a(iv)). The samples were photopolymerized with UV light (peak wavelength of λ = 365 nm) with a power density of 10 mWcm^{-2} for 10 min. Once the film had been fully cross-linked, a scalpel was used to detach one of the four corners of the sample (Figure 5a(v)). After removing the top glass substrate of the sample, the free-standing film was then extracted from the bottom glass layer with a razor blade and tweezers. An example of a free-standing film is presented in Figure 5a(vi). Figure 5c(i) shows a photograph of the LC free-standing film captured with a digital single lens reflex (SLR) camera. The films were first attached to a glass substrate for an initial observation on a POM before being removed and then transferred to a mechanically adjustable slit for further characterization.

2.3. Characterization of the Stretchable Phase Gratings

To observe the phase gratings directly, the patterned free-standing film was positioned on a glass substrate (Figure 5a(vii)) and placed on a POM. An image of the phase grating can be seen in Figure 5b. Figure 5b(i),(ii) show the grating before and after the delimitation, respectively. It can be seen that the overall width of each grating shrinks a little bit from the initial value (768 µm), which indicates that the film contracts during the delamination process and therefore might be slightly thicker than 20 µm. The reason for this is that the detachment of the film decreases the internal pressure within the LC gel forcing it to shrink and become thicker to compensate for this pressure decrease.

In order to determine the mechanical tunability of the stretchable phase grating after bulk UV curing and delamination, the patterned film was placed across an adjustable mechanical slit consisting of two metallic plates whose separation could be altered using a micrometer (Thorlabs), as shown in Figure 5c(ii). By adjusting the micrometer setting, the separation between the metallic plates could be varied resulting in either an extension or relaxation of the LC film. The slit was initially set to have a separation of 1.30 mm, which was then increased in step sizes of 0.05 mm until the film was eventually broken so that the full tunable range could be determined [59,60]. To test the reversibility in terms of successive extensions and contractions of the film, the free-standing films were stretched to an extent that would not lead to the films being broken. By comparing the tunable characteristics of the film before and after relaxation, the reversibility could be determined.

To complement the direct observations of the grating on a POM, measurements of the diffraction patterns observed in the far-field were also recorded in replay imaging system, which is shown in Supplementary Figures S3 and S4. In this case, the separation of the metallic plates on which the film was placed was varied and a laser diode operating at λ = 635 nm was incident on the diffraction grating. A white screen placed at 23 cm from the sample in the far-field allowed us to observe the diffraction pattern and a full-color Thorlabs CCD camera (DCC1240C) was used to record images of the diffraction pattern in order to determine the relative intensities in each diffraction order. By measuring the spatial separation between the zeroth and 1st order spots, r, the grating period, d, can be estimated from

$$d = \frac{a\lambda}{r} \tag{1}$$

where a represents the distance between the diffraction grating and the screen in the replay field. Here, we have used the standard grating equation, $d \sin\theta_m = m\lambda$, ($m$ is an integer representing the diffraction order of interest) and employed the small angle approximation, $\sin\theta \approx \tan\theta = \frac{r}{a}$). By tracking the change in the separation r as the film is either extended or contracted, we can determine the change in the grating period and compare this with our observations on the microscope.

3. Results and Discussion

3.1. Demonstration of a Laser-Written Diffraction Grating in a Free-Standing LC Gel

As mentioned previously, the grating contains 65 polymer walls spaced at 12 μm, which results in a total grating width of 768 μm after the laser writing process. However, a film formulation of 30 wt.%-RM257 would typically shrink to around 94% of the original size after delamination, as can be seen in Figure 6a, which shows that the grating is now 723 μm in length. From the enlarged image, the dark stripes show the laser written polymer walls which have locked-in a homeotropic alignment of the LC director. The remaining non-laser written regions, on the other hand, have been exposed to UV illumination for bulk polymerization. Figure 6b represents the corresponding diffraction pattern of the phase grating in the far field. Results for the intensities in the different diffraction orders are shown in Figure 6c.

Simulations were conducted to predict the intensity profile of the different orders in the diffraction pattern and to compare the results from simulations with the results from the experiments [55,61–63]. To model the phase grating, the tilt angle of the LC director was determined from simulations for both the laser written regions that have frozen-in a homeotropic alignment due to the application of a high voltage (100 Vrms) during fabrication and the regions in between the laser written walls that have been stabilized by UV illumination with no voltage applied (0 Vrms). For the simulations, we have assumed that the thickness of the film was 20 μm, the initial pre-tilt angle to be 4^0, the grating period to be 12 μm, and the birefringence of the LC mixture to be Δn = 0.17 (n_e = 1.71, n_o = 1.54). We also applied the one-constant approximation for the elastic constants (i.e., $K_{11} = K_{22} = K_{33} = K$ = 11.6 pN). By determining the director orientation in both the laser written and UV aligned regions this enables the periodic optical phase difference after the

grating to be simulated so that the diffraction pattern in the far-field can be determined using a fast Fourier transform (FFT) as shown in Figure 6d.

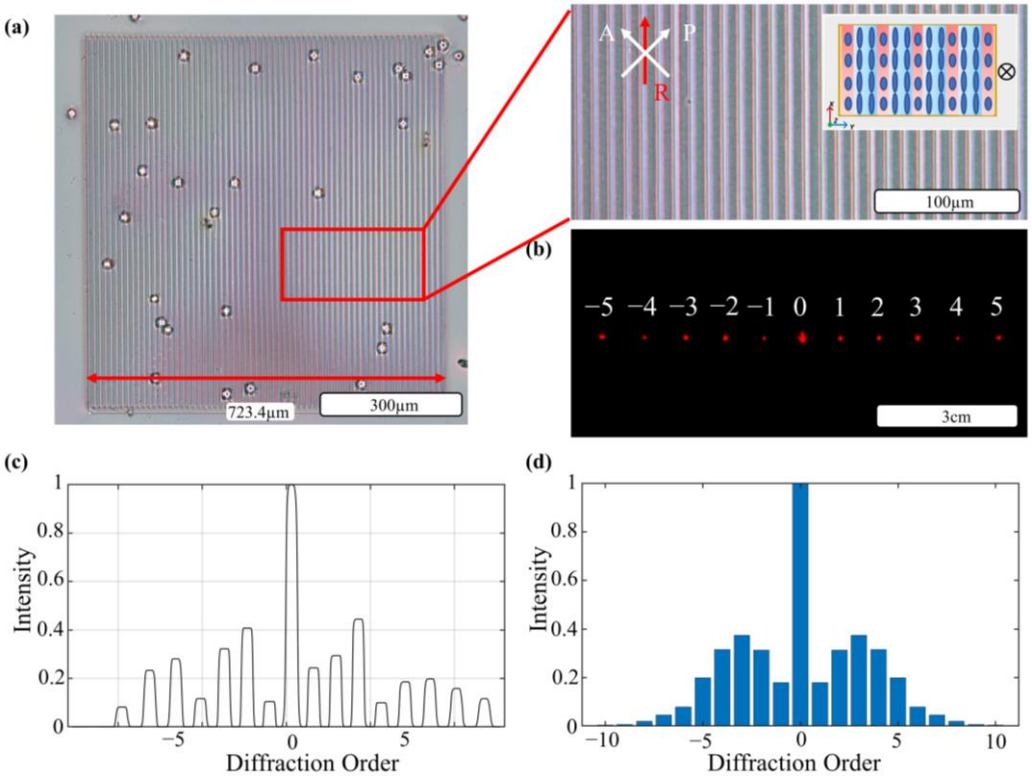

Figure 6. Characteristics of a laser-written diffraction grating in a free-standing LC film. (**a**) Polarizing optical microscope (POM) and (**b**) replay field images after delamination of the film. The white arrows labelled P and A refer to the orientations of the polarizer and analyzer, respectively, and the red arrow labelled R represents the rubbing direction of the alignment layers in the glass cell. (**c**) Experimental results of the intensity profile for the different diffraction orders. The results have been normalized to the value of the intensity of the zeroth order. (**d**) Simulated normalized intensity distribution for the free-standing film in the replay field after delamination.

For the phase grating in the free-standing film, the intensity profile predicted by simulation does agree, to some extent, qualitatively with the experimental intensity distribution recorded by the CCD camera as shown in Figure 6c. However, the experimental intensity distribution shows some degree of asymmetry that is not replicated in the simulations. One potential reason for this is that the LC director is biased in one direction because of the pre-tilt at the substrate surfaces. This biasing of the LC director could result in the asymmetry observed in the intensities recorded in the far-field diffraction pattern. In the experiments, the sample is relatively thick (20 μm); however, for the simulations, the sample is considered to be thin in accordance with Raman-Nath diffraction, which assumes that the propagation path is straight across the bulk of the film and any variation in direction is ignored. Supplementary Figure S5a shows the director tilt as a function of both the position throughout the bulk and the position within each grating period, while (b) represents the retardance distribution induced by the laser written grating with a period of 12 μm without and with a voltage of 100 Vrms applied, respectively. It confirms the LC phase grating can be fabricated by the TPP-DLW system not only from the perspective of simulations but also from that of polarization measurements. The images in Figure S5b were captured using a Mueller matrix microscope [64–66].

3.2. Tuning the Grating Period

Figure 7a shows POM images of the two extreme cases in terms of stretching: the initial unperturbed grating and the grating when the film was stretched. The film was stretched from a length of 724 ± 3 µm to 825 ± 3 µm, resulting in a change in grating period from 11.31 ± 0.05 µm to 12.89 ± 0.05 µm, which indicates that the film can be stretched by 114% of its initial length. Figure 7b shows the change in the diffraction pattern in the far-field as the film is stretched resulting in a decrease in the spacing between successive orders. From these images, the intensities of each diffraction order were tracked by the CCD camera and are shown in the plot presented in Figure 7c as the film was stretched. During the stretching process, the separation between the zeroth order and either of the first orders decreases from 13.0 mm to 11.4 mm, which corresponds to a change in the grating period from 11.3 ± 0.2 µm to 12.9 ± 0.2 µm. This result is in very good agreement with the results obtained from the POM images for the change in grating period for the same extension of the film. It was found that as the film was extended, the intensity in the zeroth order decreased dramatically while the intensity in the first order increased.

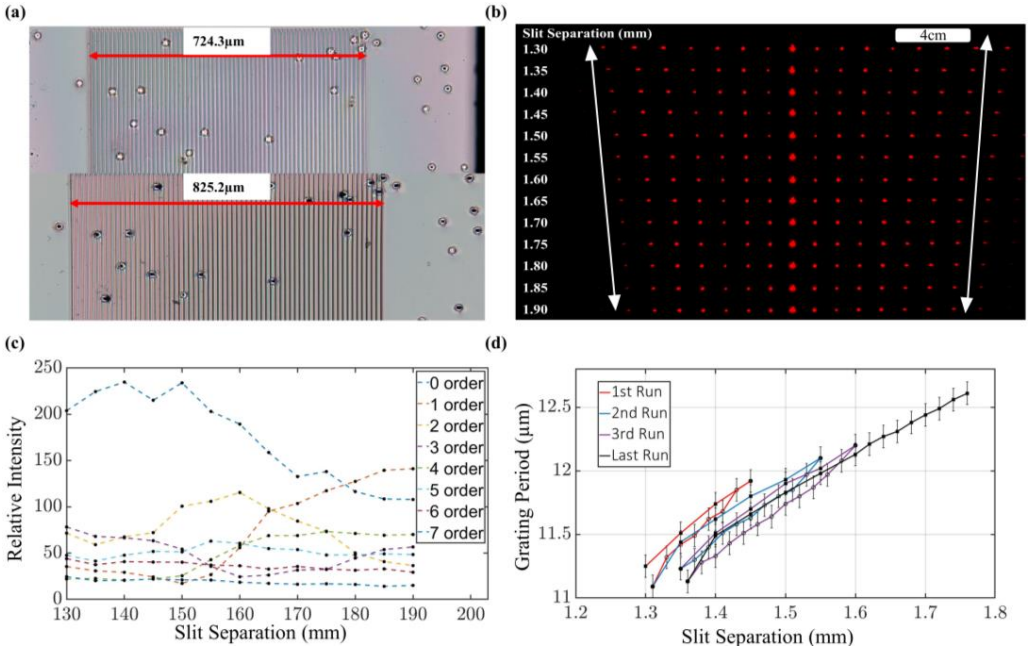

Figure 7. Mechanically tuning the 1D diffraction grating. (**a**) Polarization optical microscope (POM) images which show the grating in the undistorted state and the grating after the film has been extended by the maximum amount. (**b**) Replay field images which show the change in the diffraction pattern observed in the far-field as the grating is extended and contracted. (**c**) Intensity of each diffraction order as a function of slit separation. The dashed lines between the measured values are to guide the eye only and the estimated error in these relative intensity measurements is ±4%. (**d**) Grating period as a function of the separation between the metal plates (the slit) on which the samples were placed and which triggered either an extension or contraction of the film. The values for the grating period were obtained from POM images. Solid squares represent an extension of the film while open circles indicate a contraction of the film.

The film was stretched by varying the opening of the slit in step sizes of 0.05 mm upon increasing the separation and step sizes of 0.02 mm upon decreasing the separation of the slit. This process was repeated three times until the film was stretched to the point that it was broken. Figure 7d presents results of the grating period determined from the POM images as a function of the separation of the slit on the adjustable mount (which in turn causes an extension of the film). The results show that the grating period can be returned to its original size before being stretched again, demonstrating the elastic behavior and reversibility of the free-standing film. Specifically, the grating period returns to the same

value (between 11.10 μm and 11.30 μm). As shown in Supplementary Figure S6, the results for the stretchability and reversibility obtained from the far-field measurements appear to be in good agreement with the results obtained from the POM images.

The dependence of the grating period on the slit separation follows a roughly linear dependence. In Figure 7d, the gradients for each of these lines of best fit appear to be approximately the same, which means the film can contract back to its previous size for the same slit separation as before. Therefore, it indicates that the film did not slide too much during the stretching and contraction processes. According to the experimental data, the film only slid on the slit by 0.05 mm during the whole process. The replay field images obtained for the stretching and contraction process can be found in Supplementary Figure S6. Supplementary Figure S7 shows two extremes in terms of stretching.

3.3. Comparison of the Laser Written and UV Polymerization Regions

In order to investigate the difference in the mechanical stretchability between the laser written diffraction grating and the surrounding UV-polymerized regions that had not been subjected to laser writing, the locations of the 20-micron spacer beads trapped in the film were tracked during the stretching process. It was noticed that whenever the film was contracted, the gratings appeared to shrink more than the regions of the polymerized LC that did not consist of laser written gratings. This indicated that the polymer network formed in the laser-written regions appeared to be more rigid than those in the non-written UV-illuminated regions. By tracking the positions of the spacer beads at various locations in the film during the stretching process, the different 'stretchability' for the different regions could be evaluated.

Figure 8 presents the results obtained when six spacer beads randomly distributed through the film were monitored during the stretching process. A–F represent the six spacer beads (Figure 8a) that were tracked with image processing while the film was subjected to a mechanical strain to elongate the film in a direction parallel to the grating period. Since the gradient of the straight line fit in Figure 8b is smaller than unity, under the same force, the strain of AB is larger than that of EF, which verifies the assumption that the pure polymer film is 'softer' than the high-voltage laser written region. Therefore, the stiffness of polymer network fabricated with the laser writing at a high voltage is a bit larger than that observed for UV bulk curing, which indicates that the elasticity of the film in the different regions is not the same. In Figure 8c, the distance between C and D remains the same while the film was subjected to a mechanical stress. This means that the film does not show any deformation along an axis perpendicular to the direction in which the film is being extended. Therefore, the stretchable LC film only elongates in the direction parallel to the applied force. This would allow one to deform the sample in two dimensions separately, providing a potential route to the development of sophisticated 2D-gratings that exhibit different tuning characteristics if elongated along different directions. In order to ensure that the volume remain unchanged, the film thickness must reduce.

3.4. A Stretchable 2D Diffraction Grating

To conclude, we also demonstrate the feasibility of mechanically tuning more complex 2-dimensional diffraction gratings. Dammann gratings play a key role as optical array generators as they can uniformly distribute the optical energy among the designed diffraction orders. Conventional Dammann gratings are binary-phase gratings that generate equal-intensity spot arrays. Generally speaking, they cannot be tuned continuously. However, the mechano-optical approach presented here could potentially lead to analogue tuning of the grating. As an example, the laser written pattern in Figure 9a was designed to have a specific phase profile such that it leads to a diffraction pattern consisting of a 2-d array of 6×6 spots in the form of a rhombus shape. Based upon the stretchability achieved demonstrated herein, the initial angles of the rhombus in Figure 9a were set to be 84° and 96°. When the film was subjected to a mechanical stress, the rhombus shape in Figure 9a then gradually transformed into a square with angles of 90° and 90°, respectively, at maximum

strain. Similarly, the diffraction pattern altered from a diamond shape to a square array during stretching (Figure 9b shows the diffraction pattern before and after stretching). It can be seen that the separation between each laser spot in the horizontal direction contracts resulting in the array of spots forming a square arrangement. The repeatability of this specific device was not investigated in detail. However, we believe that as the formulation and the fabrication process are the same as that used for the film presented in Figure 7d (with the exception that this one is a more sophisticated grating) we would expect this 2-D stretchable grating film to display a similar level of repeatability in terms of an extension and contraction of the film. Mechanically tuning complex 2D diffraction elements is of potential importance for tunable AR/VR devices, tunable multiple imaging processes, mechanical beam steering and next generation optical sensors.

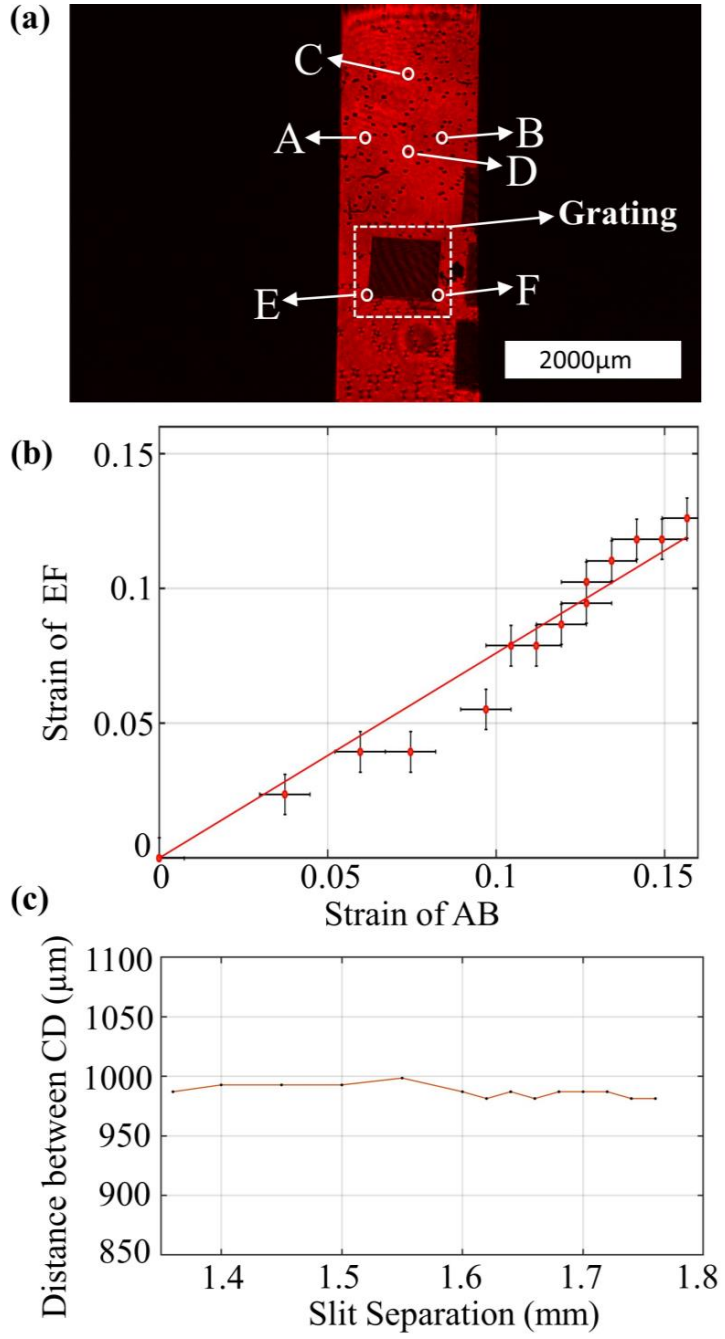

Figure 8. Comparison of the stiffness of the polymer network in either the laser written or UV polymerized regions in the stretchable films. (**a**) Photograph of the stretchable film when illuminated

with a 635 nm laser diode and captured with the CCD camera. The six spacer beads are labelled A–F. By tracking the separation between A & B and E & F as the film is stretched, the relationship between the strain for the region occupied by the (laser written) grating and that of the surrounding (UV polymerized) film can be determined. (**b**) The strain for the region between E and F as a function of the strain experienced for the region between A and B. The red line represents a line of best fit. (**c**) Separation between spacer beads C and D as a function of the slit separation. The red line is to guide the eye.

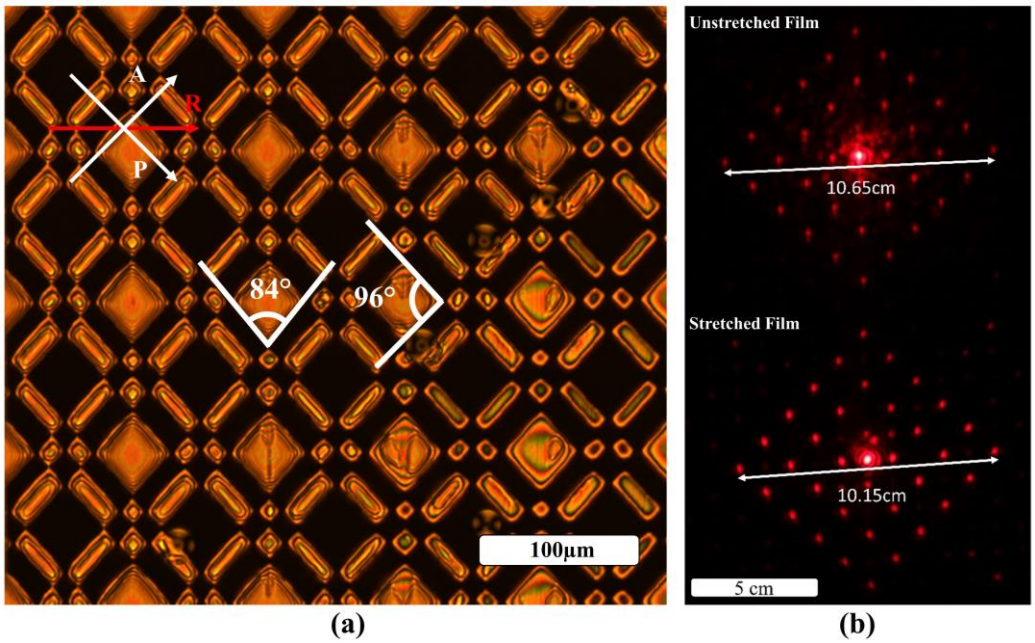

Figure 9. Demonstration of mechanical stretching of a free-standing laser written film with a 2D diffraction pattern in the far-field. (**a**) a POM image of a film (20 µm) with a laser written 6 × 6 2D Dammann grating in a rhombus shape. The dark regions correspond to the homeotropic aligned director locked-in using TPP-DLW at a voltage of 100 Vrms, while the bright regions correspond to the domains of the LC gel photopolymierzed using UV exposure without an electric field; (**b**) Far-field images of the change in the diffraction pattern in the replay field before stretching and when the film was stretched.

4. Conclusions

In summary, we have proposed and demonstrated tunable one- and two-dimensional phase gratings written in thin (20 µm-thick) LC gels that have been patterned with a combination of TPP-DLW and bulk UV illumination. These phase gratings can be mechanically tuned by subjecting the gels to an external tensile strain along the grating period. Results are also presented that show the mechanical tuning of the far-field diffraction pattern of a 2D Dammann grating which gradually changes from a rhombus shape to a square shape. These results confirm that the mechanical tunability could be applied to other tunable diffractive optical elements; for example, continuously tunable holograms. It was shown that a patterned free-standing LC gel consisting of a mixture of 30 wt.% RM257 and the nematic LC E7 can be stretched by 14% of its initial size leading to a change in the grating period of approximately 2 microns. This tuning of the grating period was verified both by observing changes in the diffraction grating directly on a POM and by tracking the change in the separation of the diffraction orders in the far-field. In addition, results were obtained that indicated there was a difference in the mechanical strength between the laser written and non-written regions by tracking the movement of the spacer beads that were trapped in the LC gel. The results indicated that the UV-illuminated polymerized regions were softer than the laser-written regions within the gratings, and that the film did not deform along an axis orthogonal to the direction in which the films were stretched. These

results demonstrate the important potential of mechano-optical diffractive optic elements that have been fabricated in LC gels using both laser writing and UV to form polymer networks. Improvements in the mixture formulation will ensure that larger tuning ranges can be achieved in the future.

Supplementary Materials: The following supporting information can be downloaded at: https://www.mdpi.com/article/10.3390/cryst12101340/s1, Figure S1. Schematic of the optical layout of the two-photon polymerisation direct laser writing system. The main subsystems are highlighted by dashed rectangular frames. The red lines refer to the path of excitation for the two-photon absorption (TPA) process at λ = 780 nm as the beam from the Ti:Sapphire laser propagates to the LC samples. The yellow path represents the illumination of the sample and image capture with the CCD camera. Figure S2. (a) Schematic of the experimental setup used to record the transmission of monochromatic light through the polymerizable LC when sandwiched between crossed polarisers. ND: neutral density filter; PD: photodiode. The light from the laser first travels through a polarizer used to provide linear polarised light before the beam is attenuated by a variable neutral density (ND) filter (Thorlabs NDC-50C-4). The beam then propagates to the LC sample and through an analyzer that is crossed with respect to the first polariser before the intensity is then recorded by a photodiode. The LC sample was positioned at 45° respect to each one of the polarizers. (b) Normalized transmission as a function of voltage for the LC mixture. The transmission decreases to zero when the sample is subjected to a voltage amplitude of 100 Vrms corresponding to a homeotropic alignment of the LC director. Figure S3. Schematic of the optical setup for characterizing the diffractive optical elements. The red solid line in the optical path represents the emission from the laser diode (λ = 635 nm), while the purple dashed line indicates the illumination path from the LED light source with a central wavelength of λ = 660 nm. Figure S4. (a) An example photograph showing the diffraction gratings in the LC when observed using the system presented in Figure S3 with the LED source turned on. (b) An example photograph of the sample when the LED was switched off and the laser diode (used to observe the diffraction pattern) was turned on. (c) An example photograph showing the LC sample when both the LED and the laser diode were switched on. This enables the position of the laser beam relative to the laser-written diffraction grating to be determined. (d) A photograph of the experiment whereby the far-field diffraction pattern can be seen on a white screen. Figure S5. (a) The tilt in the LC director as a function of position within the cross section of a grating period. This shows that the LC director is tilted at $\pi/2$ within the laser written regions but relaxes to a non-homeotropic alignment within the regions intended to be polymerized using UV illumination. (b) The retardance distribution of a laser written grating in an LC sample before UV polymerization and delamination. The image on the left represents the phase retardance induced by the grating with a period of 12 μm without an applied voltage while the image on the right shows the retardance when a voltage of 100 Vrms is applied to the LC. According to the comparison of the retardance distribution without and with a voltage, it's notable that the laser writing process locked-in a periodic phase profile which functions as a phase grating when no voltage is applied but that the grating vanishes when a large voltage was applied. Figure S6. Photographs of the polarizing optical microscope (a) and the replay field (b) for all the extremes in terms of stretching and contracting the film for the three separate cycles. In (a), the fourth order spots are linked by solid white lines to highlight the tuning and reversibility of the film. (b) represents the polarizing optical microscope images which are correspond to relevant far field images. In both methods, it can be observed that the diffraction grating is stretched further after each contraction. Figure S7. Comparison between the initial diffraction pattern and the final extreme in terms of stretching. Table S1. Fabrication parameters in the laser written gratings test.

Author Contributions: Conceptualization, B.C., S.M.M., S.J.E., M.J.B. and P.S.S.; methodology, B.C., Z.Z., C.N., C.H., S.J.E., P.S.S., M.J.B. and S.M.M.; validation, B.C., Z.Z., C.N.,C.H. and S.J.E.; formal analysis, B.C., Z.Z., C.N.,C.H. and S.J.E.; investigation, B.C., Z.Z., C.N., C.H., S.J.E., P.S.S., M.J.B. and S.M.M.; resources, P.S.S., S.J.E., M.J.B. and S.M.M.; data curation, B.C., Z.Z., C.N.,C.H. and S.J.E.; writing—original draft preparation, B.C., Z.Z., C.N., C.H. and S.M.M.; writing—review and editing, B.C., Z.Z., C.N., C.H., S.J.E., P.S.S., M.J.B. and S.M.M.; supervision, S.M.M., S.J.E., M.J.B., C.H. and P.S.S.; project administration, S.M.M. and S.J.E.; funding acquisition, S.M.M., P.S.S., S.J.E. and M.J.B. All authors have read and agreed to the published version of the manuscript.

Funding: This research was part-funded by EPSRC in the UK: grant EP/R004803/01 (EPSRC Fellowship Patrick Salter), grant EP/R511742/1 for an Impact Acceleration project, and grant EP/T517811/1 (a CASE Conversion studentship award with Merck Ltd. for Camron Nourshargh). This research was also supported by the John Fell Fund (Oxford University Press) and The Royal Society (UK) who provided resources for the laser writing facility.

Data Availability Statement: The data presented in this study are openly available in Oxford University Research Archive at 10.5287/bodleian:E92K24a4P, reference number 508697.

Conflicts of Interest: The authors declare no conflict of interest.

References

1. Bonod, N.; Neauport, J. Diffraction Gratings: From Principles to Applications in High-Intensity Lasers. *Adv. Opt. Photonics* **2016**, *8*, 156. [CrossRef]
2. Goncharsky, A.; Goncharsky, A.; Durlevich, S. Diffractive Optical Element for Creating Visual 3D Images. *Opt. Express* **2016**, *24*, 9140. [CrossRef]
3. Levola, T. Diffractive Optics for Virtual Reality Displays. *J. Soc. Inf. Disp.* **2006**, *14*, 467. [CrossRef]
4. Xiong, J.; Yin, K.; Li, K.; Wu, S.-T. Holographic Optical Elements for Augmented Reality: Principles, Present Status, and Future Perspectives. *Adv. Photonics Res.* **2021**, *2*, 2000049. [CrossRef]
5. Loewen, E.G. Diffraction Gratings for Spectroscopy. *J. Phys. E* **1970**, *3*, 201. [CrossRef]
6. He, Z.; Gou, F.; Chen, R.; Yin, K.; Zhan, T.; Wu, S.-T. Liquid Crystal Beam Steering Devices: Principles, Recent Advances, and Future Developments. *Crystals* **2019**, *9*, 292. [CrossRef]
7. Lightman, S.; Bin-Nun, M.; Bar, G.; Hurvitz, G.; Gvishi, R. Structuring Light Using Solgel Hybrid 3D-Printed Optics Prepared by Two-Photon Polymerization. *Appl. Opt.* **2022**, *61*, 1434. [CrossRef]
8. Blanchard, P.M.; Fisher, D.J.; Woods, S.C.; Greenaway, A.H. Phase-Diversity Wave-Front Sensing with a Distorted Diffraction Grating. *Appl. Opt.* **2000**, *39*, 6649. [CrossRef]
9. He, J.; Kovach, A.; Wang, Y.; Wang, W.; Wu, W.; Armani, A.M. Stretchable Optical Diffraction Grating from Poly(Acrylic Acid)/Polyethylene Oxide Stereocomplex. *Opt. Lett.* **2021**, *46*, 5493. [CrossRef]
10. Münchinger, A.; Hahn, V.; Beutel, D.; Woska, S.; Monti, J.; Rockstuhl, C.; Blasco, E.; Wegener, M. Multi-Photon 4D Printing of Complex Liquid Crystalline Microstructures by in Situ Alignment Using Electric Fields. *Adv. Mater. Technol.* **2022**, *7*, 2100944. [CrossRef]
11. Del Pozo, M.; Delaney, C.; Bastiaansen, C.W.M.; Diamond, D.; Schenning, A.P.H.J.; Florea, L. Direct Laser Writing of Four-Dimensional Structural Color Microactuators Using a Photonic Photoresist. *ACS Nano* **2020**, *14*, 9832–9839. [CrossRef] [PubMed]
12. Wang, Y.; Li, Z.; Xiao, J. Stretchable Thin Film Materials: Fabrication, Application, and Mechanics. *J. Electron. Packag.* **2016**, *138*, 020801. [CrossRef]
13. He, Y.; Gao, L.; Bai, Y.; Zhu, H.; Sun, G.; Zhu, L.; Xu, H. Stretchable Optical Fibre Sensor for Soft Surgical Robot Shape Reconstruction. *Opt. Appl.* **2021**, *51*, 589–604. [CrossRef]
14. Tham, N.C.Y.; Sahoo, P.K.; Kim, Y.-J.; Murukeshan, V.M. Ultrafast Volume Holography for Stretchable Photonic Structures. *Opt. Express* **2019**, *27*, 12196. [CrossRef] [PubMed]
15. Xu, M.-J.; Huang, Y.-S.; Ni, Z.-J.; Xu, B.-L.; Shen, Y.-H.; Guo, M.-Q.; Zhang, D.-W. Two-Dimensional Stretchable Blazed Wavelength-Tunable Grating Based on PDMS. *Appl. Opt.* **2020**, *59*, 9614. [CrossRef]
16. Yin, K.; Lee, Y.-H.; He, Z.; Wu, S.-T. Stretchable, Flexible, Rollable, and Adherable Polarization Volume Grating Film. *Opt. Express* **2019**, *27*, 5814. [CrossRef]
17. Simonov, A.N.; Akhzar-Mehr, O.; Vdovin, G. Light Scanner Based on a Viscoelastic Stretchable Grating. *Opt. Lett.* **2005**, *30*, 949. [CrossRef]
18. Oh, J.Y.; Rondeau-Gagné, S.; Chiu, Y.-C.; Chortos, A.; Lissel, F.; Wang, G.-J.N.; Schroeder, B.C.; Kurosawa, T.; Lopez, J.; Katsumata, T.; et al. Intrinsically Stretchable and Healable Semiconducting Polymer for Organic Transistors. *Nature* **2016**, *539*, 411–415. [CrossRef]
19. Tee, B.C.K.; Ouyang, J. Soft Electronically Functional Polymeric Composite Materials for a Flexible and Stretchable Digital Future. *Adv. Mater.* **2018**, *30*, 1802560. [CrossRef]
20. Kim, K.; Park, Y.; Hyun, B.G.; Choi, M.; Park, J. Recent Advances in Transparent Electronics with Stretchable Forms. *Adv. Mater.* **2019**, *31*, 1804690. [CrossRef]
21. Wang, Y.; Liu, X.; Li, S.; Li, T.; Song, Y.; Li, Z.; Zhang, W.; Sun, J. Transparent, Healable Elastomers with High Mechanical Strength and Elasticity Derived from Hydrogen-Bonded Polymer Complexes. *ACS Appl. Mater. Interfaces* **2017**, *9*, 29120–29129. [CrossRef] [PubMed]
22. Brown, D.H.; Das, V.; Allen, R.W.K.; Styring, P. Monodomain Liquid Crystal Elastomers and Elastomeric Gels: Improved Thermomechanical Responses and Phase Behaviour by Addition of Low Molecular Weight LCs. *Mater. Chem. Phys.* **2007**, *104*, 488–496. [CrossRef]
23. Biggins, J.S.; Warner, M.; Bhattacharya, K. Elasticity of Polydomain Liquid Crystal Elastomers. *J. Mech. Phys. Solids* **2012**, *60*, 573–590. [CrossRef]

24. Khosla, S.; Lal, S.; Tripathi, S.K.; Sood, N.; Singh, D. Optical Properties of Liquid Crystal Elastomers. *Am. Inst. Phys.* **2011**, *1393*, 303–304.
25. Shahinpoor, M. Electrically Activated Artificial Muscles Made with Liquid Crystal Elastomers. In Proceedings of the Smart Structures and Materials 2000: Electroactive Polymer Actuators and Devices (EAPAD), New Port Beach, CA, USA, 6–8 March 2000; p. 187.
26. Yu, Y.; Nakano, M.; Ikeda, T. Liquid-Crystalline Elastomers with Photomechanical Properties. In Proceedings of the Optical Science and Technology, the SPIE 49th Annual Meeting, Denver, CO, USA, 2–6 August 2004; p. 1.
27. DeSimone, A.; Gidoni, P.; Noselli, G. Liquid Crystal Elastomer Strips as Soft Crawlers. *J. Mech. Phys. Solids* **2015**, *84*, 254–272. [CrossRef]
28. Xie, P.; Zhang, R. Liquid Crystal Elastomers, Networks and Gels: Advanced Smart Materials. *J. Mater. Chem.* **2005**, *15*, 2529. [CrossRef]
29. Urayama, K. Selected Issues in Liquid Crystal Elastomers and Gels. *Macromolecules* **2007**, *40*, 2277–2288. [CrossRef]
30. Li, M.-H.; Keller, P. Artificial Muscles Based on Liquid Crystal Elastomers. *Philos. Trans. R. Soc. A Math. Phys. Eng. Sci.* **2006**, *364*, 2763–2777. [CrossRef]
31. Wei, R.B.; Zhang, H.; He, Y.; Wang, X.; Keller, P. Photoluminescent Nematic Liquid Crystalline Elastomer Actuators. *Liq. Cryst.* **2014**, *41*, 1821–1830. [CrossRef]
32. Geiger, S.; Michon, J.; Liu, S.; Qin, J.; Ni, J.; Hu, J.; Gu, T.; Lu, N. Flexible and Stretchable Photonics: The Next Stretch of Opportunities. *ACS Photonics* **2020**, *7*, 2618–2635. [CrossRef]
33. Chen, W.; Liu, W.; Jiang, Y.; Zhang, M.; Song, N.; Greybush, N.J.; Guo, J.; Estep, A.K.; Turner, K.T.; Agarwal, R.; et al. Ultrasensitive, Mechanically Responsive Optical Metasurfaces via Strain Amplification. *ACS Nano* **2018**, *12*, 10683–10692. [CrossRef]
34. Simonov, A.N.; Grabarnik, S.; Vdovin, G. Stretchable Diffraction Gratings for Spectrometry. *Opt. Express* **2007**, *15*, 9784. [CrossRef] [PubMed]
35. Yin, D.; Feng, J.; Ma, R.; Zhang, X.-L.; Liu, Y.-F.; Yang, T.; Sun, H.-B. Stability Improved Stretchable Metallic Gratings with Tunable Grating Period in Submicron Scale. *J. Light. Technol.* **2015**, *33*, 3327–3331. [CrossRef]
36. Yin, K.; Lee, Y.; He, Z.; Wu, S. Stretchable, Flexible, and Adherable Polarization Volume Grating Film for Waveguide-based Augmented Reality Displays. *J. Soc. Inf. Disp.* **2019**, *27*, 232–237. [CrossRef]
37. Mahpeykar, S.M.; Xiong, Q.; Wei, J.; Meng, L.; Russell, B.K.; Hermansen, P.; Singhal, A.V.; Wang, X. Stretchable Hexagonal Diffraction Gratings as Optical Diffusers for In Situ Tunable Broadband Photon Management. *Adv. Opt. Mater.* **2016**, *4*, 1106–1114. [CrossRef]
38. Xu, L.; Liu, N.; Ge, J.; Wang, X.; Fok, M.P. Stretchable Fiber-Bragg-Grating-Based Sensor. *Opt. Lett.* **2018**, *43*, 2503. [CrossRef]
39. Ghisleri, C.; Potenza, M.A.C.; Ravagnan, L.; Bellacicca, A.; Milani, P. A Simple Scanning Spectrometer Based on a Stretchable Elastomeric Reflective Grating. *Appl. Phys. Lett.* **2014**, *104*, 061910. [CrossRef]
40. Kowerdziej, R.; Ferraro, A.; Zografopoulos, D.C.; Caputo, R. Soft-Matter-Based Hybrid and Active Metamaterials. *Adv. Opt. Mater.* **2022**, *28*, 2200750. [CrossRef]
41. Sakellari, I.; Yin, X.; Nesterov, M.L.; Terzaki, K.; Xomalis, A.; Farsari, M. 3D Chiral Plasmonic Metamaterials Fabricated by Direct Laser Writing: The Twisted Omega Particle. *Adv. Opt. Mater.* **2017**, *5*, 1700200. [CrossRef]
42. Chi, T.; Somers, P.; Wilcox, D.A.; Schuman, A.J.; Johnson, J.E.; Liang, Z.; Pan, L.; Xu, X.; Boudouris, B.W. Substituted Thioxanthone-Based Photoinitiators for Efficient Two-Photon Direct Laser Writing Polymerization with Two-Color Resolution. *ACS Appl. Polym. Mater.* **2021**, *3*, 1426–1435. [CrossRef]
43. Sandford O'Neill, J.; Salter, P.; Zhao, Z.; Chen, B.; Daginawalla, H.; Booth, M.J.; Elston, S.J.; Morris, S.M. 3D Switchable Diffractive Optical Elements Fabricated with Two-Photon Polymerization. *Adv. Opt. Mater.* **2022**, *10*, 2102446. [CrossRef]
44. Li, G.; Lee, D.; Jeong, Y.; Cho, J.; Lee, B. Holographic Display for See-through Augmented Reality Using Mirror-Lens Holographic Optical Element. *Opt. Lett.* **2016**, *41*, 2486. [CrossRef]
45. Katz, S.; Kaplan, N.; Grossinger, I. Using Diffractive Optical Elements: DOEs for Beam Shaping-Fundamentals and Applications. *Laser Tech. J.* **2018**, *13*, 83–86.
46. Del Pozo, M.; Delaney, C.; Pilz da Cunha, M.; Debije, M.G.; Florea, L.; Schenning, A.P.H.J. Temperature-Responsive 4D Liquid Crystal Microactuators Fabricated by Direct Laser Writing by Two-Photon Polymerization. *Small Struct.* **2022**, *3*, 2100158. [CrossRef]
47. Del Pozo, M.; Sol, J.A.H.P.; Schenning, A.P.H.J.; Debije, M.G. 4D Printing of Liquid Crystals: What's Right for Me? *Adv. Mater.* **2022**, *34*, 2104390. [CrossRef]
48. McCracken, J.M.; Tondiglia, V.P.; Auguste, A.D.; Godman, N.P.; Donovan, B.R.; Bagnall, B.N.; Fowler, H.E.; Baxter, C.M.; Matavulj, V.; Berrigan, J.D.; et al. Microstructured Photopolymerization of Liquid Crystalline Elastomers in Oxygen-Rich Environments. *Adv. Funct. Mater.* **2019**, *29*, 1903761. [CrossRef]
49. Ku, K.; Hisano, K.; Kimura, S.; Shigeyama, T.; Akamatsu, N.; Shishido, A.; Tsutsumi, O. Environmentally Stable Chiral-Nematic Liquid-Crystal Elastomers with Mechano-Optical Properties. *Appl. Sci.* **2021**, *11*, 5037. [CrossRef]
50. Kizhakidathazhath, R.; Higuchi, H.; Okumura, Y.; Kikuchi, H. Effect of Polymer Backbone Flexibility on Blue Phase Liquid Crystal Stabilization. *J. Mol. Liq.* **2018**, *262*, 175–179. [CrossRef]
51. Vaezi, M.; Seitz, H.; Yang, S. A Review on 3D Micro-Additive Manufacturing Technologies. *Int. J. Adv. Manuf. Technol.* **2013**, *67*, 1721–1754. [CrossRef]

52. Dierking, I. Polymer Network-Stabilized Liquid Crystals. *Adv. Mater.* **2000**, *12*, 167–181. [CrossRef]
53. Baldacchini, T. *Three-Dimensional Microfabrication Using Two-Photon Polymerization: Fundamentals, Technology, and Applications*; William Andrew: Norwich, NY, USA, 2015; ISBN 9780323354059.
54. Do, M.T.; Li, Q.; Nguyen, T.T.N.; Benisty, H.; Ledoux-Rak, I.; Lai, N.D. High Aspect Ratio Submicrometer Two-Dimensional Structures Fabricated by One-Photon Absorption Direct Laser Writing. *Microsyst. Technol.* **2014**, *20*, 2097–2102. [CrossRef]
55. Tartan, C.C.; Sandford O'Neill, J.J.; Salter, P.S.; Aplinc, J.; Booth, M.J.; Ravnik, M.; Morris, S.M.; Elston, S.J. Read on Demand Images in Laser-Written Polymerizable Liquid Crystal Devices. *Adv. Opt. Mater.* **2018**, *6*, 1800515. [CrossRef]
56. Sandford O'Neill, J.J.; Salter, P.S.; Booth, M.J.; Elston, S.J.; Morris, S.M. Electrically-Tunable Positioning of Topological Defects in Liquid Crystals. *Nat. Commun.* **2020**, *11*, 2203. [CrossRef]
57. Zhao, Z.; Chen, B.; Salter, P.S.; Booth, M.J.; O'Brien, D.; Elston, S.J.; Morris, S.M. Multi-Element Polychromatic 2-Dimensional Liquid Crystal Dammann Gratings. *Adv. Mater. Technol.* **2022**. [CrossRef]
58. Woska, S.; Münchinger, A.; Beutel, D.; Blasco, E.; Hessenauer, J.; Karayel, O.; Rietz, P.; Pfleging, S.; Oberle, R.; Rockstuhl, C.; et al. Tunable Photonic Devices by 3D Laser Printing of Liquid Crystal Elastomers. *Opt. Mater. Express* **2020**, *10*, 2928. [CrossRef]
59. Wood, S.M.; Castles, F.; Elston, S.J.; Morris, S.M. Wavelength-Tuneable Laser Emission from Stretchable Chiral Nematic Liquid Crystal Gels via in Situ Photopolymerization. *RSC Adv.* **2016**, *6*, 31919–31924. [CrossRef]
60. Castles, F.; Morris, S.M.; Hung, J.M.C.; Qasim, M.M.; Wright, A.D.; Nosheen, S.; Choi, S.S.; Outram, B.I.; Elston, S.J.; Burgess, C.; et al. Stretchable Liquid-Crystal Blue-Phase Gels. *Nat. Mater.* **2014**, *13*, 817–821. [CrossRef]
61. Deshmukh, R.R.; Jain, A.K. Effect of Anti-Parallel and Twisted Alignment Techniques on Various Propertiesof Polymer Stabilised Liquid Crystal (PSLC) Films. *Liq. Cryst.* **2016**, *43*, 436–447. [CrossRef]
62. Harvey, J.E.; Pfisterer, R.N. Understanding Diffraction Grating Behavior: Including Conical Diffraction and Rayleigh Anomalies from Transmission Gratings. *Opt. Eng.* **2019**, *58*, 1. [CrossRef]
63. Harvey, J.E.; Pfisterer, R.N. Understanding Diffraction Grating Behavior, Part II: Parametric Diffraction Efficiency of Sinusoidal Reflection (Holographic) Gratings. *Opt. Eng.* **2020**, *59*, 1. [CrossRef]
64. Wang, Y.; He, H.; Chang, J.; He, C.; Liu, S.; Li, M.; Zeng, N.; Wu, J.; Ma, H. Mueller Matrix Microscope: A Quantitative Tool to Facilitate Detections and Fibrosis Scorings of Liver Cirrhosis and Cancer Tissues. *J. Biomed. Opt.* **2016**, *21*, 71112. [CrossRef]
65. He, C.; He, H.; Chang, J.; Chen, B.; Ma, H.; Booth, M.J. Polarisation Optics for Biomedical and Clinical Applications: A Review. *Light Sci. Appl.* **2021**, *10*, 194. [CrossRef] [PubMed]
66. He, C.; Chang, J.; Salter, P.S.; Shen, Y.; Dai, B.; Li, P.; Jin, Y.; Thodika, S.C.; Li, M.; Tariq, A.; et al. Revealing Complex Optical Phenomena through Vectorial Metrics. *Adv. Photonics* **2022**, *4*, 026001. [CrossRef]